† Supporting Information

Modulating Ni-S Coordination in Ni_3S_2 to Promote Electrocatalytic Oxidation of 5-Hydroxymethylfurfural at Ampere-Level Current Density

Lan Chen, ‡[ab] Zhaohui Yang, ‡[c] Chuanyu Yan,[ab] Yijun Yin,[c] Zhimin Xue,*[ab] Yiting Yao,[ab] Shao Wang,[c] Fanfei Sun,*[de] Tiancheng Mu*[c]

[a.] Beijing Key Laboratory of Lignocellulosic Chemistry, Beijing Forestry University, Beijing 100083, China. E-mail: zmxue@bjfu.edu.cn
[b.] State Key Laboratory of Efficient Production of Forest Resources, Beijing 100083, China.
[c.] School of Chemistry and Life Resources, Renmin University of China, Beijing 100872, China. E-mail: tcmu@ruc.edu.cn
[d.] Shanghai Synchrotron Radiation Facility, Shanghai Advanced Research Institute, Chinese Academy of Sciences, Shanghai 201204, China. E-mail: sunff@sari.ac.cn
[e.] Shanghai Institute of Applied Physics, Chinese Academy of Sciences, Shanghai 201204, China.
[‡] These authors contributed equally.

Experimental

Materials.

5-Hydroxymethylfurfural (HMF, 99%), 2,5-furandicarboxylic acid (FDCA, 98%), 2-formyl-5-furancarboxylic acid (FFCA, 98%), 2,5-diformyfuran (DFF, 98%), 5-hydroxymethyl-2-furancarboxylic acid (HMFCA, 98%), nickel nitrate ($Ni(NO_3)_2 \cdot 6H_2O$, 99%), and ammonium formate (90%) were obtained from Sigma-Aldrich. Ethyl alcohol (99%), thioacetamide (TAA, 99%) and acetamide (BSA, 99%) were obtained from Innochem. Dimethylformamide (DMF, 99%) and potassium hydroxid were obtained from Energy Chemical. Nickel foam (NF, thickness 1.5 mm) was purchased from Suzhou Sinero Technology Co., Ltd., China. Methanol was of chromatographic pure grade, and the other chemicals were of analytical grade. Deionized water (DI, resistivity: ~18 MΩ·cm) was used in all experiments.

Preparation of Electrode.

The nickel foam (NF) was cut into small pieces measuring 2.0 × 3.0 cm^{-2}, and then these pieces were treated with hydrochloric acid (3.0 M), ethanol, and ultrapure water by ultrasonic washing for 10 min, respectively. Thereafter, they were dried inside a vacuum oven at 60 ^oC for 12 h.

Thioacetamide (TAA, 4 mmol) and $Ni(NO_3)_2 \cdot 6H_2O$ (2 mmol) were dissolved in a solution of 20 mL dimethylformamide (DMF) and 5 mL absolute ethanol. The mixture was transferred to a stainless-steel autoclave with Teflon-lined (30 mL). Then, a piece of clean NF was vertically inserted into the autoclave reactor and reacted at 120 ^oC for 12 h. After the autoclave reactor was naturally cooled to room temperature, the Ni_3S_2/NF was removed from the reactor and then cleaned with ultrapure water. Thereafter, it was dried inside a vacuum oven at 60 ^oC for 12 h.

Ni_3S_2/NF-0.4, Ni_3S_2/NF-0.8 and Ni_3S_2/NF-1 were prepared in a similar manner to Ni_3S_2/NF, except that the reaction solvent was changed to a ratio of water to solvent of 40%, 80% and 100%, respectively. $Ni(OH)_2$/NF was prepared in a similar manner to Ni_3S_2/NF, except that TAA was changed to BSA.

Catalyst characterization.

The scanning electron microscope (SEM) images of the samples were conducted on a field emission scanning electron microscopy (Hitachi SU 8010) coupled with energy dispersive X-ray spectroscopy operated at 15.0 kV. The transmission electron microscope (TEM) images were recorded using FEI Tecnai G2 F20 TEM. The X-ray diffraction (XRD) patterns of the samples were recorded using an X-ray diffractometer (Rigaku D/Max-2500). Data were collected in Bragg-Brettano mode using 0.02° divergence with a scan rate of 5° min^{-1}. Raman spectra of the samples were obtained using a laser confocal Raman microscope (Lab RAM Odyssey). X-ray photoelectron spectroscopic (XPS) analysis was performed by X-ray photoelectron spectrometer (Thermo Fisher K-Alpha). XAFS measurements at Ni k-edge in both transmission (for Ni foil) and fluorescence (for samples) mode were performed at Hard X-ray branch of the E-line (BL20U1) in Shanghai Synchrotron Radiation Facility (SSRF). XAFS data were

collected using a fixed-exit double-crystal Si(111) monochromator. The raw data analysis was performed using IFEFFIT software package according to the standard data analysis procedures. The Fourier transformation of the k3-weighted EXAFS oscillations, k3·χ(k), from k space to R space was performed to obtain a radial distribution function. And data fitting was done by Artemis program in IFEFFIT.

Electrochemical Measurements.

The electrochemical properties were measured by a three-electrode system using a CS350M electrochemical workstation. The reference electrode was a mercuric oxide electrode (Hg/HgO), and the counter electrode was a carbon rod. A nickel foam electrode with an area of 1 × 1 cm^2 was used as the working electrode. The Hg/HgO electrode potentials were converted to the standard hydrogen electrode (RHE) scale using E(RHE) = E(Hg/HgO) + 0.059 × pH + 0.098 V, (pH ≈ 14). Cyclic voltammetry (CV) with a scan rate of 50 $mV \cdot s^{-1}$ before the measurement was used to activate the electrodes. The scan rate for the linear voltammetric curve was 5 $mV \cdot s^{-1}$ with 70% IR compensation. The electrochemical active surface area (ECSA) was derived from the electrical double layer specific capacitor (Cdl). The Cdl values were obtained from CV curves at potentials of 0.1-0.2 V (*vs.* Hg/HgO) with a scan rate of 10-50 $mV \cdot s^{-1}$. Electrochemical impedance spectroscopy (EIS) was measured from 0.01 to 10,000 Hz using a CHI 660E electrochemical analyzer (CHInstruments, Inc., Shanghai).

Large-scale HMF electrolysis experiments were performed in a membrane electrode assembly (MEA) reactor (Figure 5e). The workstation was operated using a two-electrode system. The anodic electrolyte was 500 mL of 1 M KOH containing 50 mM HMF and the cathodic electrolyte was 100 mL of 1 M KOH. We prepared 4 cm^{-2} Ni_3S_2/NF electrocatalysts assembled at the anode and platinum sheet electrode assembled at the cathode. The electrolyte was pumped into the reaction system using a peristaltic pump. After electrolysis reaction, 1 M sulphuric acid was gradually added dropwise to the electrolyte with constant stirring until no further precipitation was produced. The product was confirmed by high performance liquid chromatography (HPLC) spectroscopy.

High performance liquid chromatography (HPLC, Shimadzu SIL-20A) with a UV-visible detector was employed to analyze the concentration of raw materials, products and intermediates in the HMFOR process. During the constant potential electrolysis with an applied potential of 1.4 V, a 10 µl sample was taken from the electrolyte when the electrolytic system passed a charge of 0, 150, 300, 450, and 578 C. The electrolyte was then acidified with 1 M sulfuric acid and diluted to 3 mL with a mixture of methanol and 5 mM ammonium formate in a ratio of 3:7. The samples were analyzed by HPLC on a 4.6 mm × 250 mm COSMOSIL 5C18-MS-II 5 µm C18 column and kept at 35 ^oC with a UV detector at 265 nm. The elution solvent was obtained by simultaneous injection of methanol and 5 mM ammonium formate in the ratio of 3:7 at a flow rate of 0.6 $mL \cdot min^{-1}$. The conversion of HMF, FDCA yield and Faraday efficiency were

calculated by the following equations, respectively, where F was Faraday's constant (96485 C/mol) and n was the number of charges transferred per mole of reaction.

$$\text{HMF conversion (\%)} = n_{\text{HMF consumption}} / n_{\text{HMF initial value}} \times 100\%$$

$$\text{FDCA yield (\%)} = n_{\text{FDCA formation}} / n_{\text{HMF initial value}} \times 100\%$$

$$\text{Faraday efficiency (\%)} = 6 \times F \times n_{\text{FDCA formation}} / \text{total charge passed} \times 100\%$$

DFT calculations.

All calculations were conducted using the Materials Studio (MS) in the Cambridge Sequential Total Energy Package (CASTEP) module. The generalized gradient approximation (GGA) functional by the Perdew-Burke-Ernzerhof (PBE) was employed. The cutoff energy was 450 eV, the pseudopotentials were OTFG ultrasoft, and the corresponding k-point sampling was 3×3×1 for geometry optimization. The Broyden-Fletcher-Goldfarb-Shanno (BFGS) scheme was selected as the minimization algorithm. The correction of van der Waals was adopt by DFT-D method of Grimme. A complete LST/QST method was used for the transition state search. A vacuum layer was set at 15 Å along the Z-axis. The convergence tolerance of energy was 2×10^{-5} eV per atom, the maximum force was 0.05 eV/Å, the maximum stress was 0.1 Gpa, and the maximum displacement was 0.002 Å.

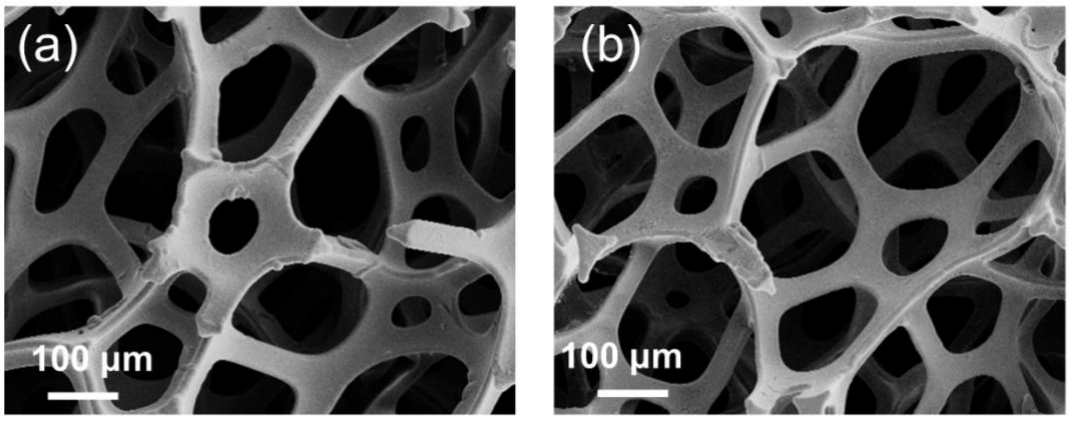

Figure S1. SEM images of (a) NF and (b) NF-after solvothermal treatment.

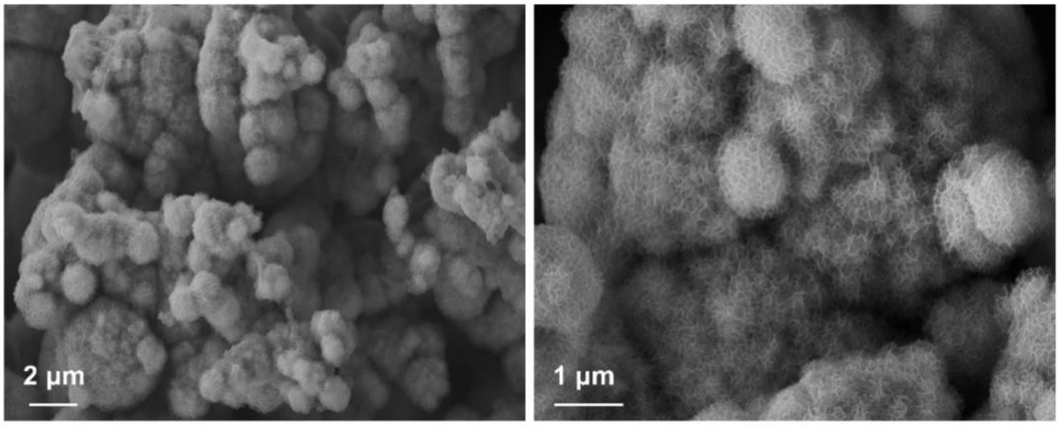

Figure S2. SEM images of Ni_3S_2/NF.

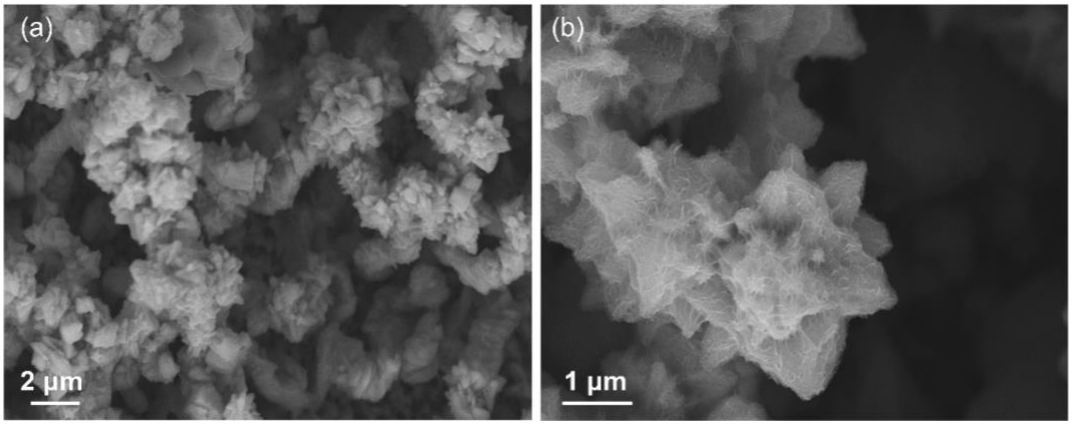

Figure S3. SEM images of Ni_3S_2/NF-0.4.

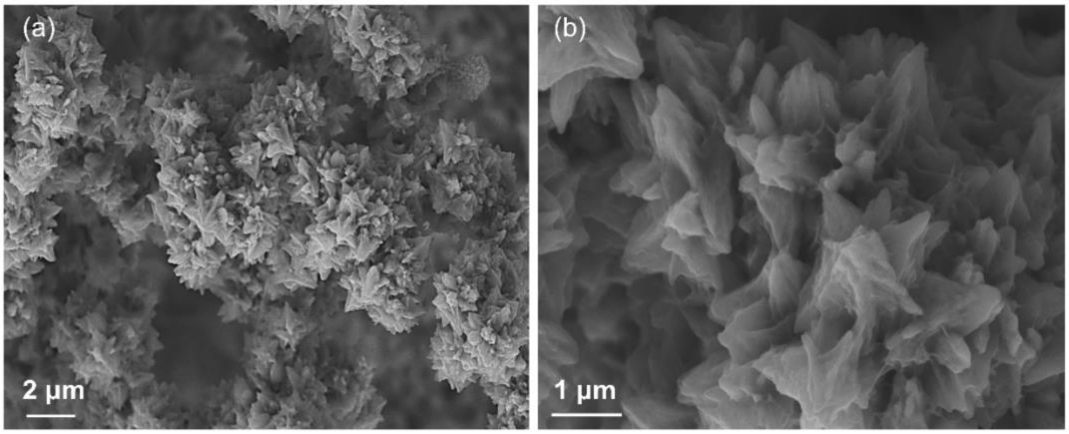

Figure S4. SEM images of Ni_3S_2/NF-0.8.

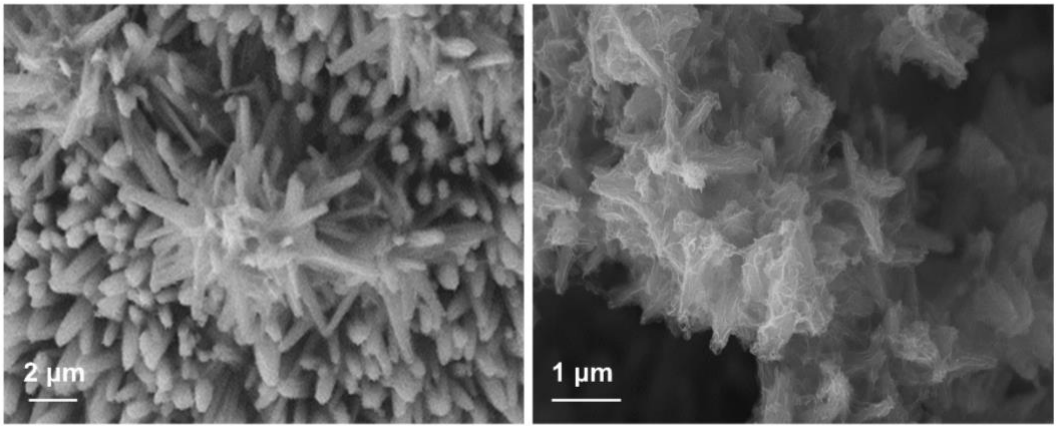

Figure S5. SEM images of Ni_3S_2/NF-1.

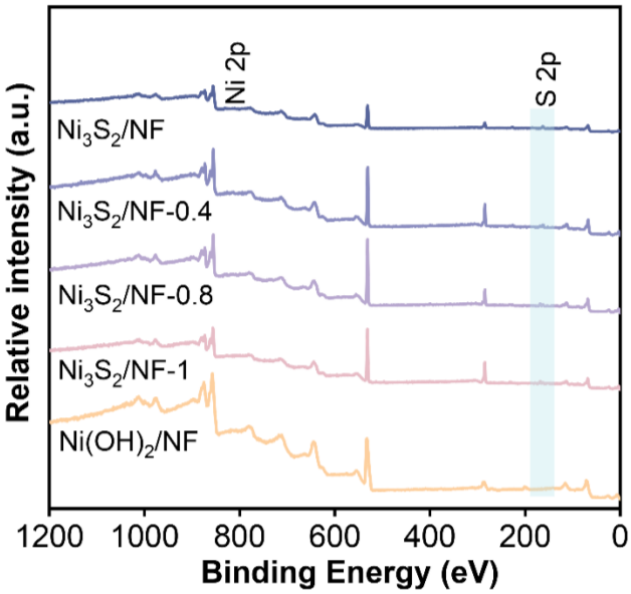

Figure S6. XPS survey spectra.

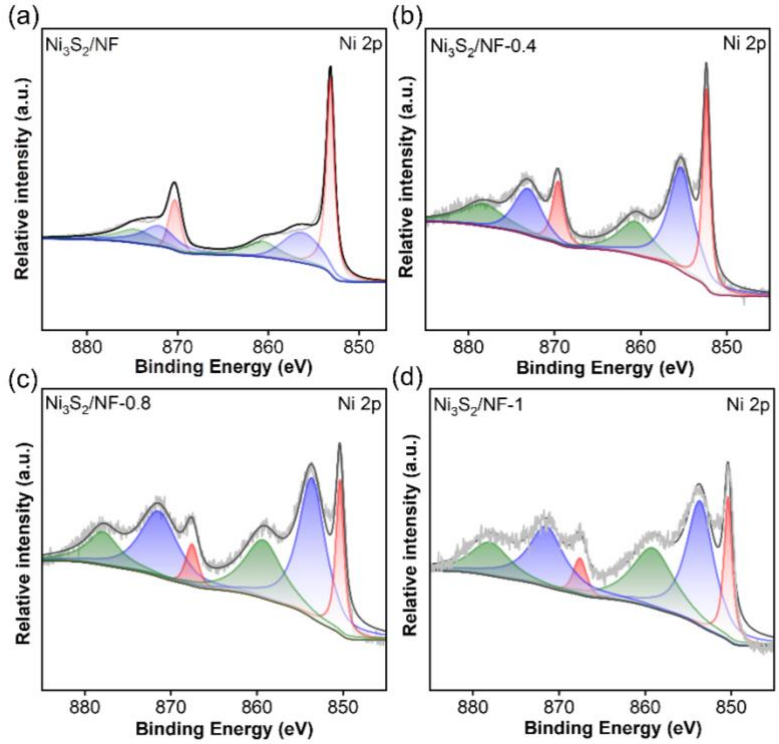

Figure S7. High-resolution XPS spectra of Ni 2p for (a) Ni_3S_2/NF, (b) Ni_3S_2/NF-0.4, (c) Ni_3S_2/NF-0.8, and (d) Ni_3S_2/NF-1 after etched by Ar+ ion for 100 s.

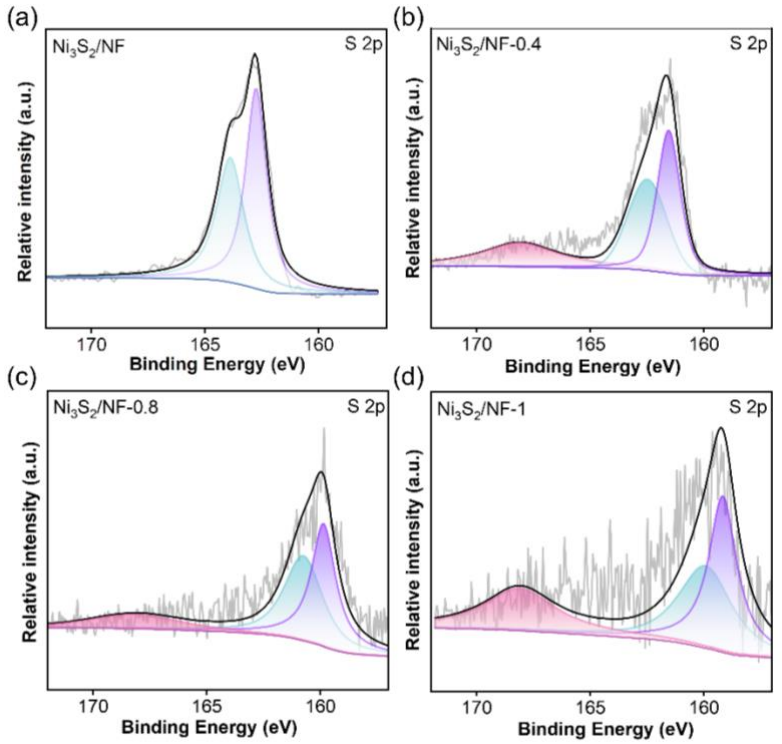

Figure S8. High-resolution XPS spectra of S 2p for (a) Ni_3S_2/NF, (b) Ni_3S_2/NF-0.4, (c) Ni_3S_2/NF-0.8, and (d) Ni_3S_2/NF-1 after etched by Ar+ ion for 100 s.

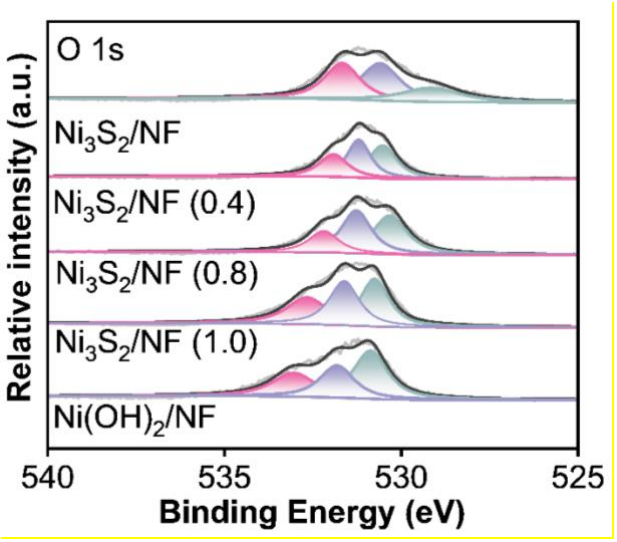

Figure S9. XPS spectra of O 1s.

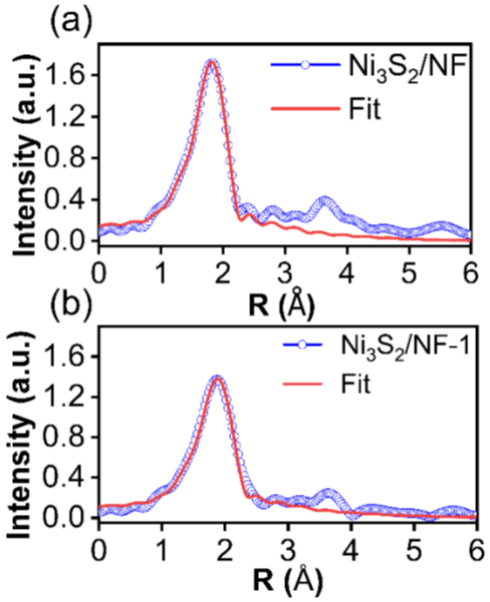

Figure S10. The EXAFS fitting curves in R-space of (a) Ni_3S_2/NF, (b) Ni_3S_2/NF-1.

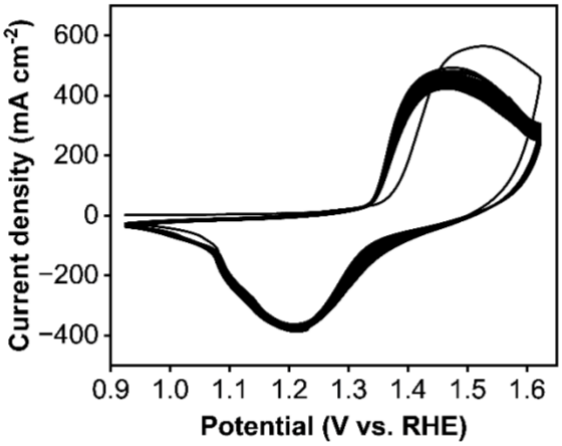

Figure S11. The cyclic voltammetry (CV) curves of Ni_3S_2/NF in 1 M KOH at a scan rate of 50 mV s^{-1}.

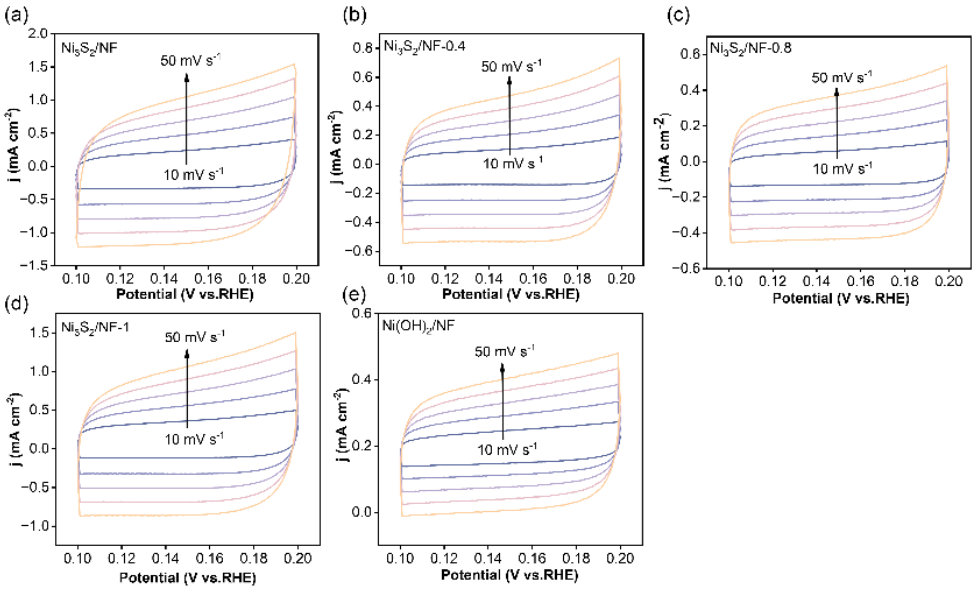

Figure S12. The polarization curves of (a) Ni_3S_2/NF, (b) Ni_3S_2/NF-0.4, (c) Ni_3S_2/NF-0.8,(d) Ni_3S_2/NF-1, and (e) $Ni(OH)_2$/NF in 1 M KOH.

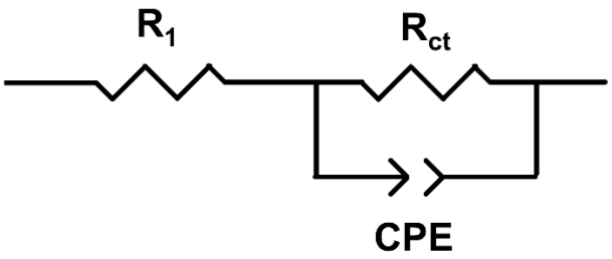

Figure S13. Equivalent circuit applied to analyze the electrochemical impedance spectroscopy. R_1 stands for the solution resistance, CPE represents double layer capacitance, and R_{ct} has contact with the interfacial charge transfer reaction.

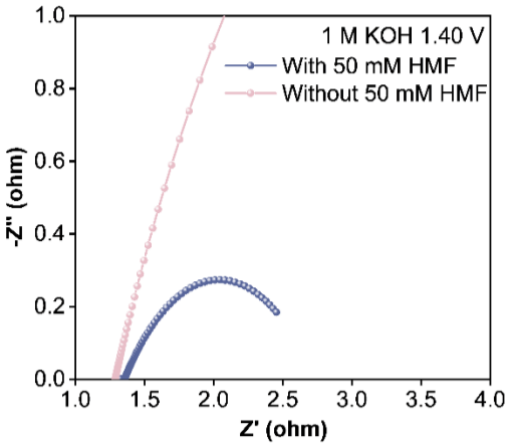

Figure S14. Nyquist plots of Ni_3S_2/NF in 1 M KOH with and without 50 mM HMF at 1.40 V vs. RHE.

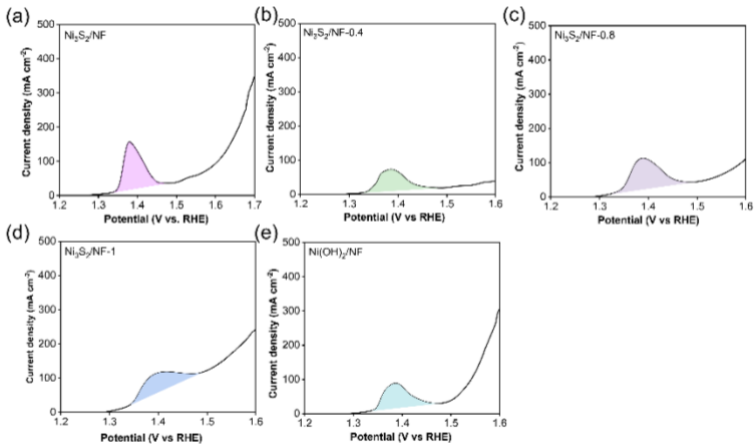

Figure S15. Integration on the Ni^{2+} to Ni^{3+} oxidation peak of (a) Ni_3S_2/NF, (b) Ni_3S_2/NF-0.4, (c) Ni_3S_2/NF-0.8,(d) Ni_3S_2/NF-1, and (e) $Ni(OH)_2$/NF.

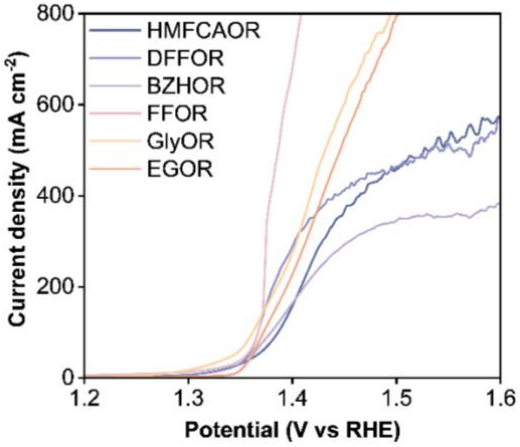

Figure S16. LSV curves of Ni_3S_2/NF for HMFCAOR, DFFOR, BZHOR, FFOR, GlyOR and EGOR.

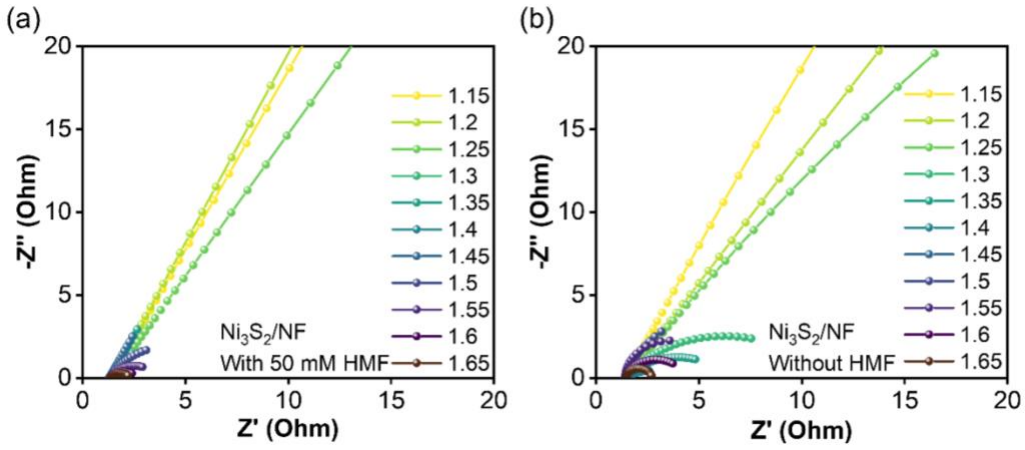

Figure S17. Nyquist plots of Ni_3S_2/NF in 1 M KOH (a) with and (b) without 50 mM HMF at various potentials.

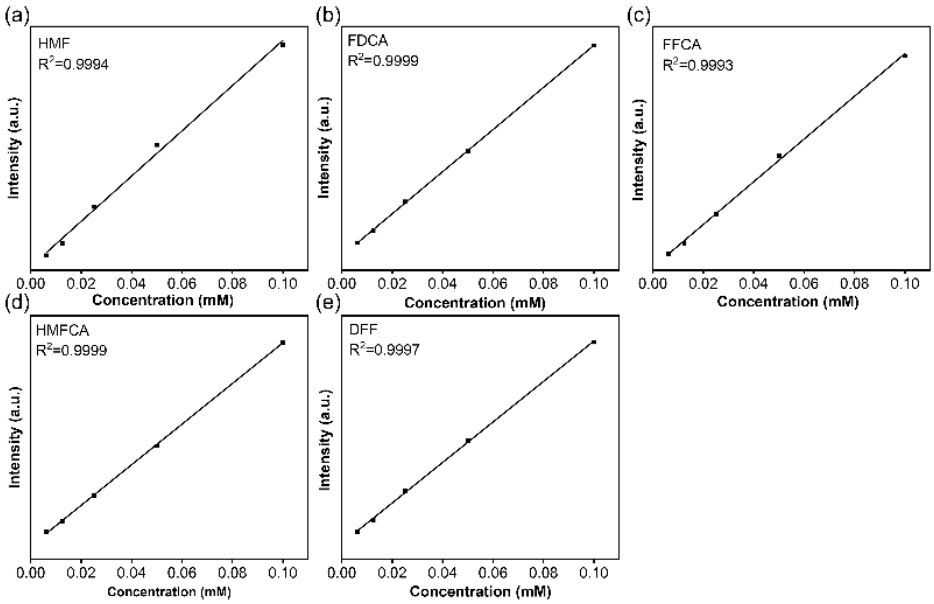

Figure S18. The standard curves of the HPLC for (a) HMF, (b) FDCA, (c) HMFCA, (d) FFCA and (e) DFF.

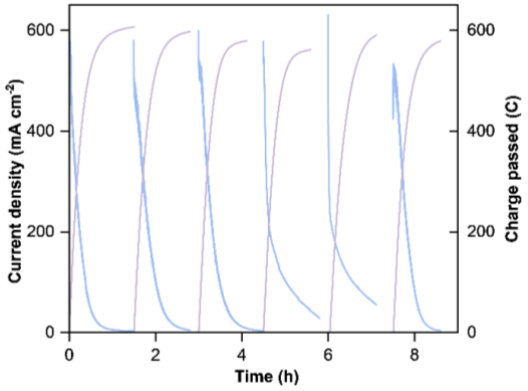

Figure S19. Current-time and charge-time curves during HMF electrooxidation at 1.4 V vs. RHE in 6 successive runs.

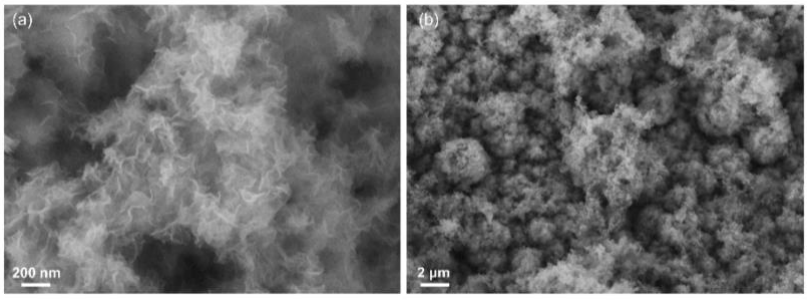

Figure S20. SEM images of Ni_3S_2/NF-used.

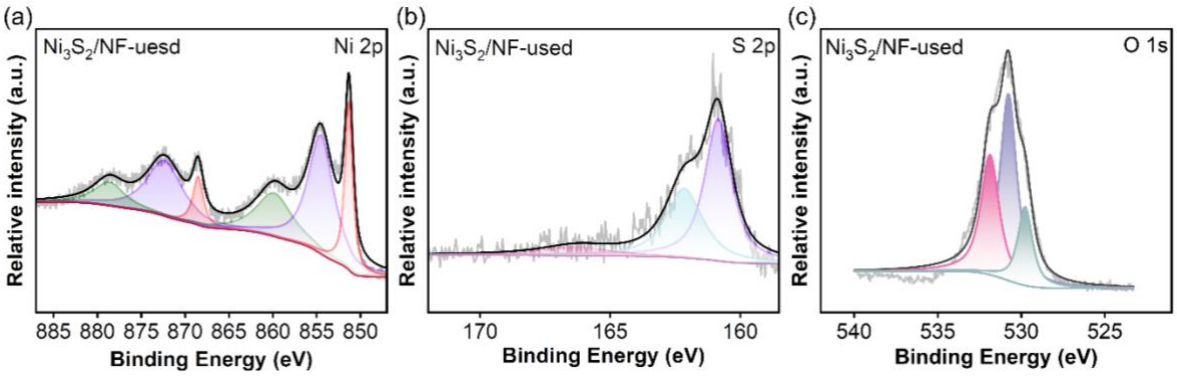

Figure S21. High-resolution XPS spectra of (a) Ni 2p, (b) S 2p and O 1s for Ni_3S_2/NF-used.

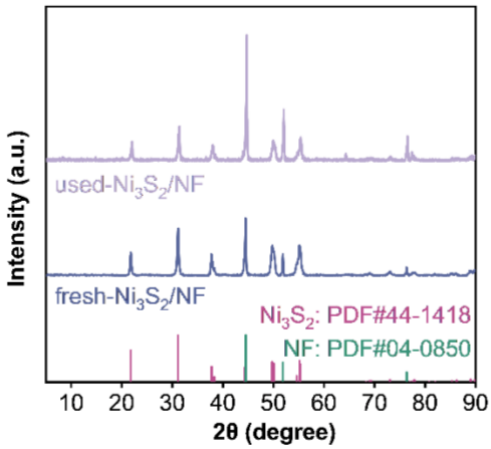

Figure S22. XRD patterns of Ni_3S_2/NF-fresh and Ni_3S_2/NF-used.

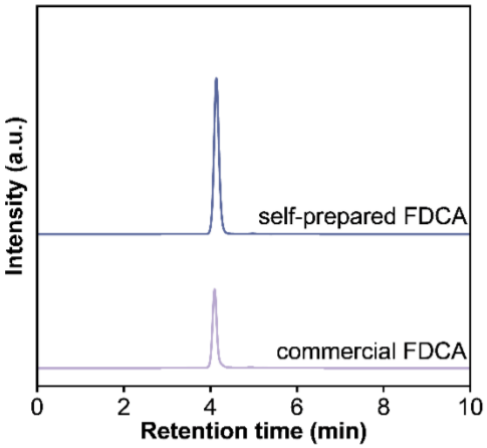

Figure S23. HPLC chromatogram traces of electrolyte during the electrochemical oxidation of (a) self-prepared FDCA and (b) commercial FDCA.

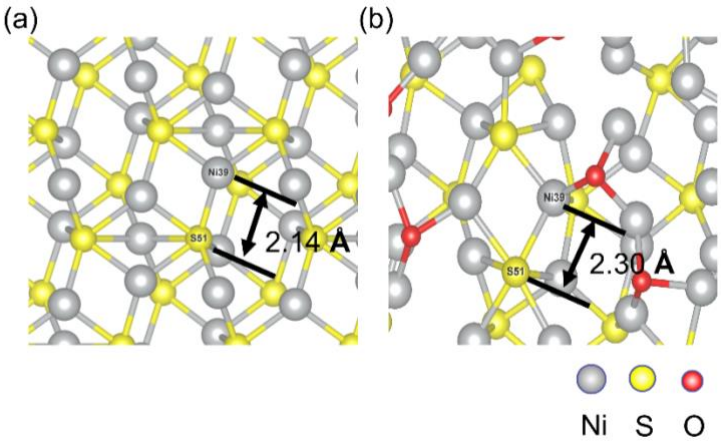

Figure S24. ICOHP values of Ni-S bonds in the Ni_3S_2/NF and Ni_3S_2/NF-1.

Table S1. The ratio of S-O/Ni-S bonds in Ni_3S_2/NF, Ni_3S_2/NF-0.4, Ni_3S_2/NF-0.8, and Ni_3S_2/NF-1.

Sample	Ratio of water in solvent (%)	ratio of S-O/Ni-S bonds
Ni_3S_2/NF	0	0
Ni_3S_2/NF-0.4	40	0.48
Ni_3S_2/NF-0.8	80	0.69
Ni_3S_2/NF-1	100	1.18

Table S2. Structural parameters extracted from the Ni K-edge EXAFS fitting data of Ni_3S_2/NF and Ni_3S_2/NF-1.

Sample	Path	N	R (Å)	ΔE_0 (eV)	$\sigma^2(10^{-3}Å^2)$
Ni_3S_2/NF	Ni-S	5.0 ± 0.3	2.28 ± 0.01	1.6 ± 0.7	8.9 ± 0.9
Ni_3S_2/NF-1	Ni-S	4.8 ± 0.5	2.35 ± 0.01	3.0 ± 1.2	10.5 ± 1.7

N is the coordination number, R is interatomic distance (the bond length between central atoms and surrounding coordination atoms), ΔE_0 is edge-energy shift (the difference between the zero kinetic energy value of the sample and that of the theoretical model), and σ^2 is Debye-Waller factor (a measure of thermal and static disorder).

Table S3. Comparison on the activities of the developed Ni_3S_2/NF and the reported ones on HMFOR.

Catalyst	Potential	Current density	Ref.
	V *vs.* RHE	$mA \cdot cm^{-2}$	
Ni_3S_2/NF	1.40	735	This work
Ni_3S_2/NF	1.45	1000	This work
Ni_3S_2/NF	1.50	1169	This work
NiS_x/β-$Ni(OH)_2$	1.36	50	[1]
Ni-Cu/NF	1.5	1000	[2]

$Co_{0.4}NiS$@NF	1.45	500	[3]
NiFe-1	1.50	630	[4]
Pt_xNi_{100-x} NWs	1.45	300	[5]
NiCoFeS-MOF	1.48	200	[6]
NiO-Ppy	1.34	100	[7]
Co-P/CF	1.423	50	[8]
Co_3O_4/CeO_2	1.50	80	[9]
Rh-O_5/Ni(Fe)	1.48	100	[10]
F-doped $NiCo_2O_4$	1.45	30	[11]

Supplementary references

[1] C. Liu, X.-R. Shi, K. Yue, P. Wang, K. Zhan, X. Wang, B.Y. Xia, Y. Yan, S-Species-Evoked High-Valence $Ni^{2+\delta}$ of the Evolved β-$Ni(OH)_2$ Electrode for Selective Oxidation of 5-Hydroxymethylfurfural, Adv. Mater., 35 (2023) 2211177.https://doi.org/10.1002/adma.202211177
[2] D. Chen, Y. Ding, X. Cao, L. Wang, H. Lee, G. Lin, W. Li, G. Ding, L. Sun, Highly Efficient Biomass Upgrading by a Ni−Cu Electrocatalyst Featuring Passivation of Water Oxidation Activity, Angew. Chem., Int. Ed., 62 (2023) e202309478.https://doi.org/10.1002/anie.202309478
[3] Y. Sun, J. Wang, Y. Qi, W. Li, C. Wang, Efficient Electrooxidation of 5-Hydroxymethylfurfural Using Co-Doped Ni_3S_2 Catalyst: Promising for H_2 Production under Industrial-Level Current Density, Adv. Sci., 9 (2022) 2200957.https://doi.org/10.1002/advs.202200957
[4] C. Wang, Y. Wu, A. Bodach, M.L. Krebs, W. Schuhmann, F. Schüth, A Novel Electrode for Value-Generating Anode Reactions in Water Electrolyzers at Industrial Current Densities, Angew. Chem., Int. Ed., 62 (2023) e202215804.https://doi.org/10.1002/anie.202215804
[5] J. Wu, Z. Kong, Y. Li, Y. Lu, P. Zhou, H. Wang, L. Xu, S. Wang, Y. Zou, Unveiling the Adsorption Behavior and Redox Properties of PtNi Nanowire for Biomass-Derived Molecules Electrooxidation, ACS Nano, 16 (2022) 21518-21526.https://doi.org/10.1021/acsnano.2c10327
[6] Y. Feng, K. Yang, R.L. Smith, X. Qi, Metal sulfide enhanced metal–organic framework nanoarrays for electrocatalytic oxidation of 5-hydroxymethylfurfural to 2,5-furandicarboxylic acid, J. Mater. Chem. A, 11 (2023) 6375-6383.https://doi.org/10.1039/D2TA09426F
[7] Y. Lu, L. Yang, Y. Jiang, Z. Yuan, S. Wang, Y. Zou, Engineering a localized electrostatic environment to enhance hydroxyl activating for electrocatalytic biomass conversion, Chin. J. Catal., 53 (2023) 153-160.https://doi.org/10.1016/S1872-2067(23)64516-4
[8] N. Jiang, B. You, R. Boonstra, I.M. Terrero Rodriguez, Y. Sun, Integrating Electrocatalytic 5-Hydroxymethylfurfural Oxidation and Hydrogen Production via Co–P-Derived Electrocatalysts, ACS Energy Lett., 1 (2016) 386-390.https://doi.org/10.1021/acsenergylett.6b00214
[9] G. Zhao, G. Hai, P. Zhou, Z. Liu, Y. Zhang, B. Peng, W. Xia, X. Huang, G. Wang, Electrochemical Oxidation of 5-Hydroxymethylfurfural on CeO_2-Modified Co_3O_4 with Regulated Intermediate Adsorption and Promoted Charge Transfer, Adv. Funct. Mater., 33 (2023) 2213170.https://doi.org/10.1002/adfm.202213170
[10] L. Zeng, Y. Chen, M. Sun, Q. Huang, K. Sun, J. Ma, J. Li, H. Tan, M. Li, Y. Pan, Y. Liu, M. Luo, B. Huang, S. Guo, Cooperative Rh-O_5/Ni(Fe) Site for Efficient Biomass Upgrading Coupled with H_2 Production, J. Am. Chem. Soc., 145 (2023) 17577-17587.https://doi.org/10.1021/jacs.3c02570
[11] S. Yang, X. Xiang, Z. He, W. Zhong, C. Jia, Z. Gong, N. Zhang, S. Zhao, Y. Chen, Anionic defects engineering of $NiCo_2O_4$ for 5-hydroxymethylfurfural

electrooxidation, Chem. Eng. J., 457 (2023) 141344.https://doi.org/10.1016/j.cej.2023.141344